



Article

# Identification of Missouri Precipitation Zones by Complex Wavelet Analysis

Jason J. Senter <sup>1</sup> and Anthony R. Lupo <sup>1,2,\*</sup>

- Atmospheric Science Program, School of Natural Resources, University of Missouri, Columbia, MO 65211, USA; jjs6qc@mail.missouri.edu
- <sup>2</sup> Missouri Climate Center, University of Missouri, Columbia, MO 65211, USA
- \* Correspondence: lupoa@missouri.edu

#### **Abstract**

Understanding the intricate dynamics of precipitation patterns is essential for effective water resource management and climate adaptation in Missouri. Existing analyses of Missouri's climate variability lack the spatial granularity needed to capture nuanced variations across climate divisions. The Missouri historical agricultural weather database, an open-source tool that contains key weather measurements gathered at Mesonet stations across the state, is beginning to fill in the data sparsity gaps. The aim of this study is to identify core patterns associated with ENSO in the global wavelet output. Using a continuous wavelet transform analysis on data from 32 stations (2000-2024), we identified significant precipitation cycles. Where previous studies used just four Automated Surface Observing Systems (ASOSs) located at airports across Missouri to characterize climate variability, this study uses an additional 28 from the Missouri Mesonet. The use of a global wavelet power spectrum analysis reveals that precipitation patterns, with the exception of southeast Missouri, have a distinct annual cycle. Furthermore, separating the stations based on the significance of their ENSO (El Niño-Southern Oscillation) signal results in the identification of three precipitation zones: an annual, ENSO, and residual zone. This spatial data analysis reveals that the Missouri climate division boundaries broadly capture the three precipitation zones found in this study. Additionally, the results suggest a corridor in central Missouri where precipitation is particularly sensitive to an ENSO signal. These findings provide critical insights for improved water resource management and climate adaptation strategies.

Keywords: Missouri; precipitation zones; continuous wavelet transform; ENSO



Academic Editors: Edoardo Bucchignani and Paul D. Williams

Received: 19 August 2025 Revised: 23 September 2025 Accepted: 30 September 2025 Published: 10 October 2025 Citation: Senter, J.J.; Lupo, A.R.

Identification of Missouri
Precipitation Zones by Complex
Wavelet Analysis. *Meteorology* **2025**, *4*,
29. https://doi.org/10.3390/
meteorology4040029

Copyright: © 2025 by the authors. Licensee MDPI, Basel, Switzerland. This article is an open access article distributed under the terms and conditions of the Creative Commons Attribution (CC BY) license (https://creativecommons.org/licenses/by/4.0/).

#### 1. Introduction

Meteorological time series measures often contain embedded complex waveform qualities. Signals within these systems may arise from both stationary and non-stationary influences, originating from local/regional or large/global-scale processes. These signals may be embedded in super-position, and standing wave forms may arise due to phase locking. Irregular and non-continuous effects in underlying signals can impact local daily precipitation measurements. This study examines the capability and benefits of augmenting data gathered from Automated Surface Observing Systems (ASOSs) operated by the National Weather Service (NWS) and located at airports with Missouri Mesonet data [1].

Meteorology **2025**, 4, 29 2 of 17

Previous studies analyzing long-term time series data for Missouri often utilized yearly or monthly temperature and precipitation from the four main NWS stations, employing Fourier analysis (e.g., [2,3]). These and other studies (e.g., [2–5]) have demonstrated a link between ENSO-related variability and temperature and precipitation data across the state, which is also reflected in staple crop yields [4]. Moreover, these broader ENSO-driven climatic variations, including jet stream displacements across North America, are known to influence a range of phenomena relevant to regional weather, such as tornado outbreaks, temperature and precipitation anomalies, storm track locations, and both tropical and extratropical circulation anomalies (e.g., [6–9]). Additionally, ENSO and other interannual variations in the general circulation are known to influence the circulation patterns and surface variables regionally for different regions of the globe, and these have been studied as well (e.g., [10–15]). Some of the above studies have examined the frequency of drought and their relationship to interannual variability (e.g., [4,5,13]). In this study, only precipitation data will be used. By augmenting the NWS data with Mesonet data, this study examines the geo-spatial organization of ENSO signal variability within precipitation across Missouri between 2000 and 2024 to better understand the potential regional implications.

Other studies have identified regional precipitation variability in local regions across the globe (e.g., [16–20]). The work of [16] used wavelet power spectra to identify annual variability within a localized region of Brazil (São Francisco River basin). Then, studies such as [17–19] examined larger regions in order to find smaller-scale regions or basins where coherent signals for precipitation variability are found on the interannual time scale and then due to ENSO or other phenomena. Also, [20] performed a similar analysis globally to identify regions that are sensitive to trends and variability in precipitation, and, in particular, how regular these patterns are and the risk they imply for local water management.

In this study, cyclic patterns are identified, and collection errors minimized using the Continuous Wavelet Transform (CWT) analysis methodology outlined in the 'Practical Wavelet Guide' [21]. The individual station analyses are spatially aggregated and visualized to assess the consistency of the composite visual representation. This study uses Missouri Mesonet data to establish a foundation for comparing how this granular data source enhances our understanding of the distribution of regional sensitivities of ENSO to precipitation across the state.

The wavelet analysis reveals multiple recurring cyclic patterns, with primary periods of approximately one and six years. Signals, also referred to as periods of interest described throughout the remainder of this document, are at or above the 95th percentile and are considered significant for this study. Some stations display up to three signals, using CWT analysis. Some stations lack any discernible signals for diagnostic use. Neither temporal continuity nor spatial homogeneity in power distribution, displayed in the scalogram, is observed in any station examined. Not only are there non-continuous properties throughout each discrete station's temporal power signal, but there exists a non-uniform spatial distribution of stations that share the ENSO signal. The distributions of shared signal patterns among stations form three primary regional clusters across the state: stations with only an annual signal, stations with both annual and ENSO signals, and stations with neither. Consequently, given this study's implication of a non-uniform spatial distribution of clustered shared signal patterns among stations across the state, precipitation predictions using ENSO measures need to consider this spatial irregularity and implement regionally specific forecasts based on the precipitation zones highlighted herein.

Meteorology **2025**, 4, 29 3 of 17

## 2. Data and Methods

## 2.1. Background: Complex Wavelet Transform

A key element of this study is to assess the cyclic nature of precipitation in Missouri. This study uses the practical wavelet guide [21] to perform a wavelet analysis to identify significant cycles in Missouri daily precipitation data to use for spatial diagnostic and comparison calculations.

This time series spectral analysis using wavelets provides a method to illustrate temporal locality, non-stationary behavior, and vacillations in duration and strength [21]. The decomposition of the time series, particularly in geophysical processes, in time–space, has allowed for the identification of low- and high-frequency phenomena consistent with the scale on which the wavelet was chosen. Consistent with previous studies, a Morlet wavelet with a central frequency (Figure 1) will serve as the band-pass filter and the "mother" wavelet for this study [21–24]. Additionally, the appropriateness of the filter shape applied to rainfall data and the Morlet wavelet's ability to capture its peaks and troughs were explored in similar studies, including earlier work on Missouri weather [2,25]. The utilization of the CWT has the advantage of providing information in a spatial context by the manipulation of a plane wave bounded in a Gaussian envelope given by

$$\psi_0(\eta) = \pi^{-\frac{1}{4}} e^{i\omega_0 \eta} e^{-\frac{\eta^2}{2}}, \ \omega_0 = 6.$$
(1)

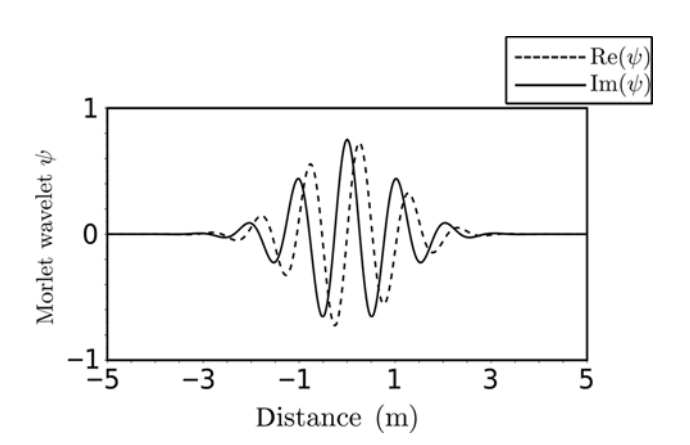


**Figure 1.** Example of the Morlet mother wavelet function, including real (dashed) and imaginary (solid) lines [22].

This continuous wave function acts as a band pass filter, generating an energy profile scaled in frequency space. The resulting 2D power spectra exhibit angular sensitivity and spatial selectivity, proportional to the selection of  $\omega_0$ . Specifically, they describe a complex sine wave at a central frequency  $\omega_0$ , which is then localized in time by being multiplied by a Gaussian envelope (the  $e^{\frac{-\eta^2}{2}}$  term). The normalized constant term  $\pi^{\frac{-1}{4}}$  was used in the wavelet procedure to fix the scaling and allow for a comparison of coefficients across different scales. The oscillatory component of the wavelet came from  $e^{i\omega_0\eta}$ , where  $\omega_0$  is the central frequency of the oscillation, and  $\eta$  is the dimensionless time parameter that allows the Morlet wavelet's fundamental shape and properties to be defined independently of the specific scale and position at which it is used to analyze a signal. The tuning procedure for  $\omega_0$ , to maximize both localization and frequency precision, was found in the Torrence and Compo guide [21]. The mother wavelet with a central frequency ( $\omega_0$ ) of 6 resulted in a balanced approach to observe the oscillation of both power and frequency over time.

Where the scalogram is a useful tool in looking for distinct power locality in time, the global wavelet spectrum is a reduction, representing power over the entire dataset. When visualized, these calculations produce a line graph where the wavelet power spectrum

Meteorology **2025**, 4, 29 4 of 17

along the confidence interval can be represented 'globally.' This global averaging over all local wavelet spectra provides a way to isolate trends over the entire time series [16].

$$\overline{W}_n^2(s) = \frac{1}{N} \sum_{n=0}^{N-1} |W_n(s)|^2$$
 (2)

In the global wavelet spectrum equation,  $\overline{W}_n^2(s)$ , s represents the wavelet scale, directly correlating with the period of the analyzed feature. Larger scales correspond to longer-term trends, while smaller scales capture more rapid fluctuations.  $W_n(s)$  denotes the local wavelet transform at a specific time point n and scale s, quantifying the presence of a particular frequency component at that moment. Squaring its magnitude,  $\overline{W}_n(s)^2$ , yields the local wavelet power spectrum, or scalogram, which indicates the energy of that frequency component at that specific time. Finally, N signifies the total number of data points in the series, ensuring that the summation encompasses the entire dataset. By averaging these local power spectra over all time points for a given scale, the global wavelet spectrum effectively filters out transient events, bringing to light significant and persistent patterns that characterize the entire time series.

#### 2.2. Dataset

The daily precipitation data used in this study came from 28 Missouri Mesonet stations and four NWS ASOS airport stations. The Mesonet data were obtained through the Missouri historical agricultural weather database, part of the University of Missouri's Extension program [1]. These data are publicly available and free to access. The four airports referenced in this study were located primarily across the middle of the state, with the exception of one, located in the southwestern part of the state, near Springfield, MO. These four airports comprised the dataset used to characterize Missouri climate measures in previous studies [3]. The daily precipitation measurements for the additional four airports were provided by the Midwest Regional Climate Center (MRCC) [26]. The stations and counties used in this study can be seen in Figure 2.

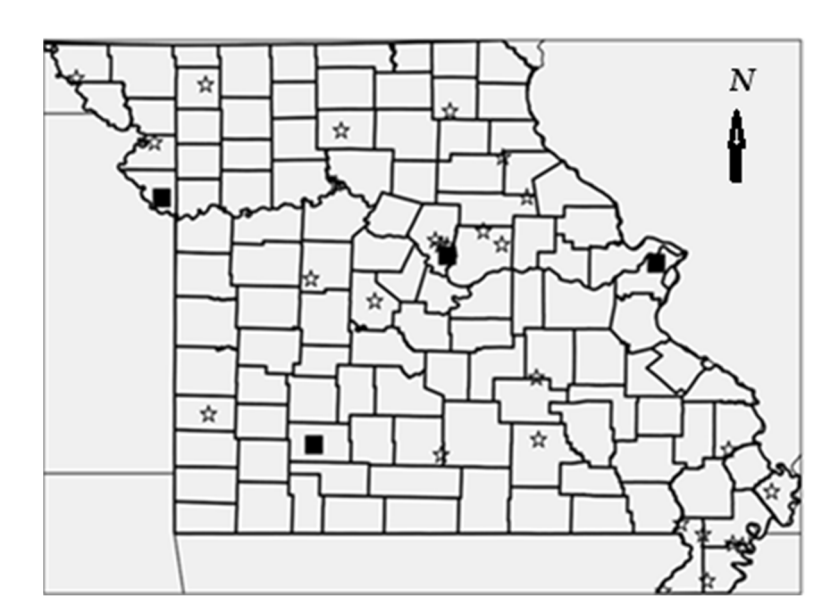


**Figure 2.** A map of the 28 Missouri Mesonet stations (stars) and four ASOS stations used in this study (solid squares). Missouri, centrally located within the conterminous United States, is a state characterized by diverse topography, including the northern plains, the Ozark Plateau to the south, and the Mississippi and Missouri River floodplains. In this map the scale is 1.75 cm = 100 km.

Meteorology **2025**, 4, 29 5 of 17

The Mesonet data provided a consistent measure of daily precipitation records year over year. The sensor located at the sites used for precipitation collection was the Campbell Scientific TE25 tipping bucket. The operating temperature for these sensors is  $0^{\circ}$  to  $50^{\circ}$ C, recording 0.01 inches (0.254 mm) per tip. The instrument's accuracy is 1%, up to 2 inches (50 mm/hr), and the gauges are placed one meter above ground within the weather station's footprint [27].

Consistent year-round precipitation measurements were a necessity for this study, despite their inherent sources of error. The Mesonet rain buckets were unheated, which potentially under-recorded accumulation due to snow blowing out of the bucket. The presence of frozen precipitation in the collection bucket also likely led to delayed reporting since the ice or snow had to melt at ambient temperatures before being measured as liquid. Accounting for these potential errors will be covered in the Section 2.3.

## 2.3. Methods

The ENSO signal has been found to modulate sensible weather in Missouri. Observing whether there was a measurable, comparable, and cogent signal in the precipitation dataset was the first goal [3]. A similar study, conducted in the São Francisco River basin, used a complex wavelet approach to identify precipitation zones and found regional consistency in their results [16]. A similar approach was used in this study to define regions of relative spatial uniformity in signal patterns over Missouri. To accomplish this, defining the individual global spectrum pattern of each station objectively prevented a biased visual composite. Consequently, this analysis yielded a direct, unmanipulated representation of the station data. This ensured minimal bias and good mapping visualization.

## 2.3.1. Data Preprocessing

First, the preprocessing of the dataset was conducted by treating missing and trace measurements as non-measurable values (zero). The precipitation data from the Mesonet is raw in nature. The interpretation has to account for biases in the design of the sensor and special consideration for the type of precipitation. Frozen precipitation with unheated sensors introduces the potential for spectral leakage due to spikes in precipitation measurements. This study did not attempt to isolate these discrete errors. One could use external present weather information and/or temperature data to generate a scheme to spread the power over the duration of the event, lowering the power. Mitigating the impact of discrete spikes and shifts is naturally handled through this wavelet procedure. Unlike a Fourier transform, the CWT allows for a mix of localization and power over time, as well as signal filtering using a Gaussian bounded wavelet. The ability to determine cyclic power fluctuations over time also allows observational dominant signal comparisons across the stations. Additionally, the wavelet acts to dampen the power associated with discrete spikes. This procedure is also designed to give the ability to discriminate against period length, allowing for the identification of annual and ENSO signals, while minimizing the potential contamination of errors on the order of the diurnal timescale.

## 2.3.2. Wavelet Configuration

The parameters for the initial survey of precipitation patterns at the Mesonet stations across the state were tuned for continuous daily data. The data were first detrended by subtracting the fitted linear trend from the original data using a polynomial of degree one. The detrended data were then normalized by dividing each value by the standard deviation, thus de-emphasizing absolute values and changes. The configuration of the 'mother' Morlet wavelet had a central frequency of 6 ( $\omega_0 = 6$ ). The time interval ( $\delta t$ ) was set to one day, and the starting scale ( $s_0$ ) was 60 days. The decision to employ a 60-day starting scale was graphically motivated, enabling a clear visualization of the low-frequency range

Meteorology **2025**, 4, 29 6 of 17

within the cone of influence (COI) on the scalogram. Consequently, this choice concurrently excluded coefficients originating from high-frequency sampling errors. The scale resolution (dj) was set to 1/12, and the number of sub-octaves (J) was computed as 7/dj, following the practical guide from Torrence and Compo [21]. A signal was considered significant if its power reached or surpassed the 95th percentile.

## 2.3.3. Station Selection Criteria

An exploratory analysis conducted after data preprocessing assessed the patterns and general behavior of each station. The analysis employed fixed wavelet parameters for comparative purposes (Figure 3). The peak period(s) was compared to the COI. For stations that had an ENSO signal, the COI had to be greater than the peak period that fell in the 2–7-year range. For this reason, only 32 of the 50 possible stations examined were utilized. Stations that were not included generally had a COI that fell below 5.5 years. An example of a borderline ENSO station classification case, with a potential ENSO signal falling above the COI, that was not used was Columbia–Capen Park. Even though it had 14 years of available data, the max period within the COI of 5.11 did not capture a 5.43-year ENSO signal. Padding the dataset could have mitigated the exclusion of this station, but because this station was co-located with other stations with clear ENSO-like signals, the omission did not distort the overall visual representation of the data over the state.

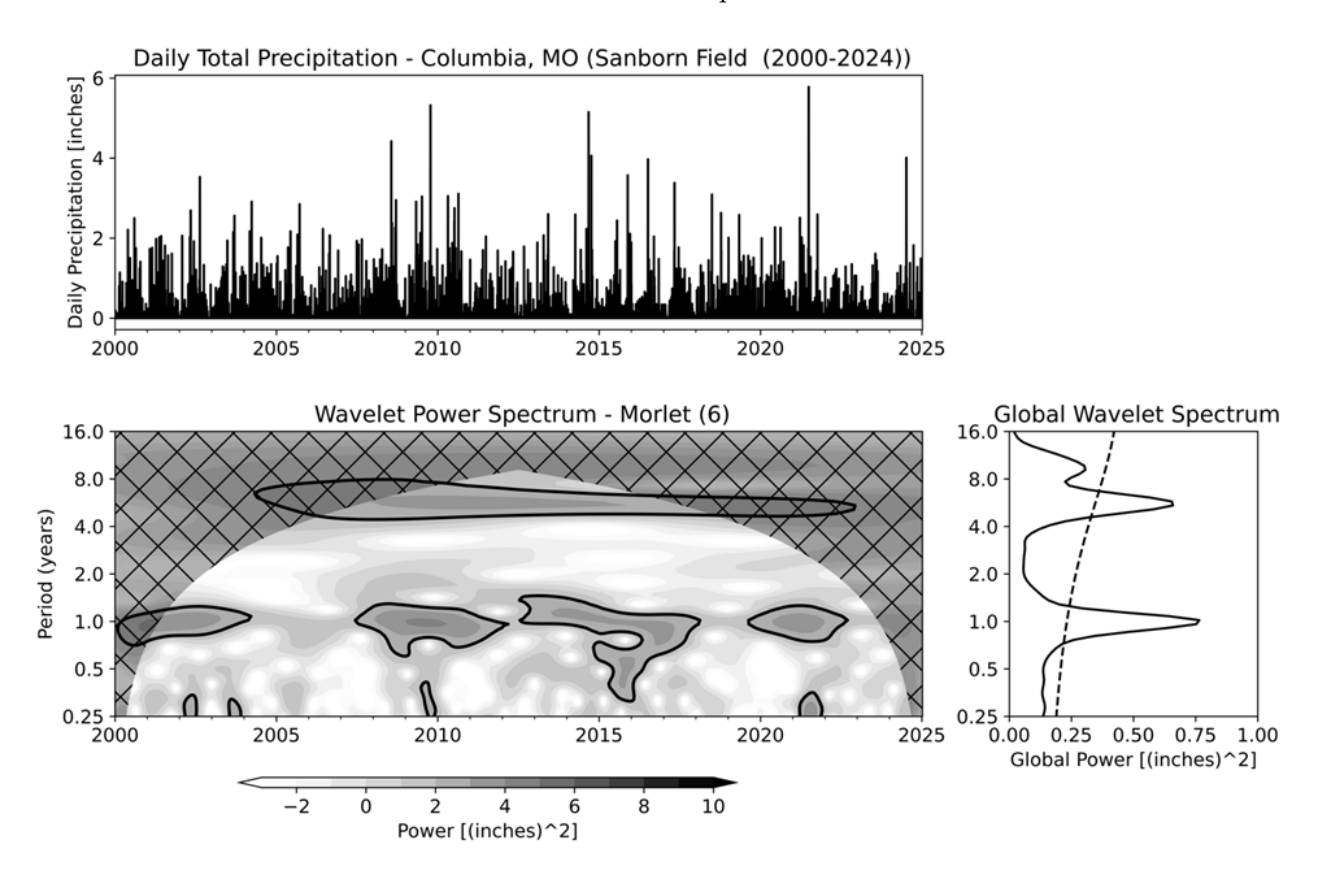


Figure 3. Daily precipitation data time series from the Sanborn Field Mesonet station (top line graph). The scalogram for the wavelet power shows periods of high and low power over time (bottom graph). The COI (hatched region) defines where edge effects become significant. The thick black contour encloses regions greater than 95% confidence for a red-noise process with an  $\alpha$  coefficient of 0.148. The global wavelet power spectrum is shown, with the 5% significance level indicated by the dashed line, calculated against a red-noise background (bottom-right line graph).

Following the exploratory analysis, a global wavelet analysis was conducted on the remaining 32 stations. Each station's peak signals were analyzed separately and Meteorology **2025**, 4, 29 7 of 17

quantitatively, to reduce subjective spatial biases. Signal strength may vary across the time series, with power often distributed non-uniformly, as seen in the power spectrum shown in Figure 3. Although the power may not be consistent, the integrated power in the global wavelet spectrum acts to synthesize the most significant cycles based on the summary power throughout the entire time series. In the case of the Mesonet precipitation data from the Sanborn Field site, there was a clear annual and ENSO signal (Figure 3). The global wavelet spectrum highlighted the dominant cycles in the entire dataset, showing the annual and ENSO patterns as distinct peaks. These peaks represented the overall strength of these cycles across all time. Even though the statistical importance of these cycles varied from year to year (as seen in the scalogram (Figure 3)), their underlying presence and influence were fundamental. After each station was analyzed, it was clear a two-step classification scheme was to be used to compress the signal types from sub-classifications A–H to just three classifications (A, B, C) found in Table 1.

**Table 1.** The two-step classification system followed first assigning a sub-classification (A–H) to the global wavelet spectrum patterns. The second step, used in the data visualization, distilled the eight unique patterns into three pattern types (A–C). (\*) Sub-classifications C and D fall under the no or residual classification.

Signal Type Classification Scheme				
Single Signal	Sub-Classification	Classification		
Annual Signal	A	A		
ENSO Signal	В	В		
Between Annual and Biennial Signal	C *	С		
Sub-Annual	D*	С		
Multiple Signals				
Annual + ENSO	E	В		
Annual + between Annual and Biennial Signal	F	A		
Annual + Sub-Annual	G	A		
None/Residuals *	Н	С		

#### 2.3.4. Two-Step Classification

The two-step classification system followed a binning scheme to isolate bin-specific characteristics found from each station's global wavelet spectrum pattern, delineating regions with a significant ENSO signal to those without an ENSO signal (e.g., [21]). The eight bins fell into three signal categories (Single, Multiple, None/Residual). For this pre-sorting step, an example of sub-classification A, used in the identification of region A, is used to describe a station that exhibits a significant annual signal. Since this study focuses on delineating regions based on annual versus ENSO sensitivity, special consideration was given to cases outside these bounds. For instance, if a station exhibited both an annual signal and other signals with periods outside the 2–7-year ENSO cycle, it was classified as "annual," potentially falling under sub-classifications F or G within classification A. An example of the classification process can be seen in Figure 4, where the A graph depicts an annual signal, B an ENSO signal along with the annual signal, and C a station void of an annual or ENSO signals. Although the stations generally had strong signals that fell into annual or ENSO buckets, the level of complexity did warrant a pre-classification to act as a pre-sorting step.

Meteorology **2025**, 4, 29 8 of 17

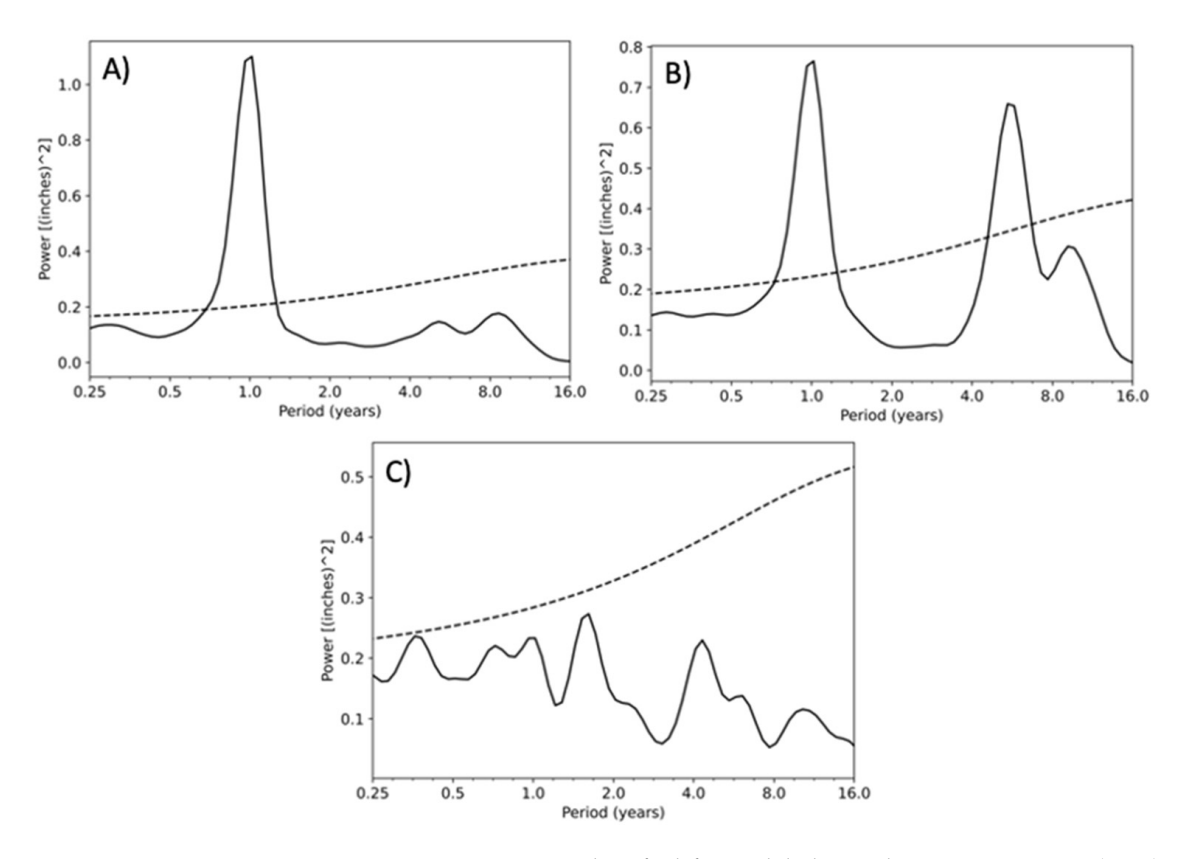


**Figure 4.** Frequency patterns identified from global wavelet power spectra: (A–C) Pattern (A) (dominant 12-month frequency), Pattern (B) (ENSO-related), and Pattern (C) (no significant frequency or residual). The abscissa represents the period in years, and the ordinate is wavelet power (unit is inch<sup>2</sup>). The solid line is wavelet power and the dashed line is the 95% confidence level.

After the pre-sorting is performed through the initial sub-classifications step, the eight patterns are distilled down to three. Within the A classification, there is a single annual signal in the single-signal category (A), an annual signal along with a signal between one and two years (F), and annual and sub-annual (G) signals. Sub-classifications within classification B are a single ENSO signal in the single-signal category (B) and an annual and ENSO signal (E) in the multiple=signal category. Sub-classifications within C denote stations with global wavelet patterns that did not fall in classifications A or B. Stations within classification C were further divided into three sub-classifications: stations with no significant signals (H), stations with a single signal between one and two years (C), and stations with a single sub-annual signal (D).

## 2.3.5. Visualization Techniques

Next, the visualization of the classification scheme is at the core of this exploratory study. Once the classifications are assigned to each station, a nearest-neighbor scheme is then used to interpolate the classifications across the state. This technique, which is a straightforward and computationally efficient method, was used to estimate values at unobserved locations based on the closest available data points. In the context of spatial data applied to the classification of precipitation zones, this technique assigns each grid cell the class value of the single nearest observed data point (station). This process involves creating a dense grid covering the area of interest and then, for every point on the grid, identifying the closest original observation point in the dataset. The class label of that closest observed point is then directly assigned to the grid cell. Consequently, the resulting interpolated map displays distinct, Voronoi-like regions where all points within a given area are classified identically to their nearest station, effectively partitioning the geographic space into zones

Meteorology **2025**, 4, 29 9 of 17

defined by the influence of the closest measurement. This method is particularly useful when discrete, exact classifications are desired, and it avoids the smoothing effects inherent in other interpolation techniques like linear or Kriging methods [28].

This method offers clear and intuitive visualization that prioritizes data integrity over esthetic enhancements common in surface interpolation approaches. The grid used was a quarter-degree grid for both interpolation and for calculating the nearest distances between the stations. Visualization of the station data centered around two mapping schemes: the four ASOS stations and the four ASOS stations along with the additional Mesonet stations. The comparison of both allowed for general remarks on using more stations along with a description of metrics underlying each sample for a more in-depth analytical assessment. The regions comprising distinct classifications were used to demarcate precipitation zones that would share the same A, B, and C identifier. The term "regions" was used interchangeably with "zones." If the regions had a mottled appearance once mapped, "zones" would then be used to further define these fragmented regions.

The interpolation scheme effectively revealed how additional stations improved spatial coverage, providing metrics such as the average nearest-neighbor distance and coverage percentage. These were calculated on a quarter-degree grid with a quarter-degree distance threshold for adjacent cells, ensuring no double-counting of overlapping grid cells. Similarly, insights into station distribution were gained from the interquartile range (IQR) of distances; this method, by focusing on the middle 50% of the data, minimized outlier influence. Consequently, the magnitude of this spread was relative to the information contained within the state's boundaries, acknowledging that peripheral stations contributed less information. Furthermore, these distance metrics were determined using geopy's geodesic function, which, in turn, implemented Vincenty's inverse formula to account for the ellipsoidal shape over the domain (Missouri) [29,30]. By taking this extra step, the domain could be accurately described, and the interpolated data clearly visualized on the uniform quarter-degree grid.

## 3. Results

This analysis highlights the utility of the Missouri Mesonet to augment spatial gaps in station coverage found from using only the four ASOS stations. Prior to this study, the spatial context of ENSO-related weather sensitivities was relegated mainly to a swath across the middle of the state. The increased spatial resolution provided by the additional Mesonet stations enhanced the robustness of this analysis. Along with the visualization comparisons between the two mapping schemes, the spatial metrics also provide a measure of fidelity from infusing the additional Mesonet data.

Through the two-part classification scheme, three distinct patterns were identified, and their visualization delineated three precipitation zones based on the global spectrum patterns. Figure 5 gives a survey of the three patterns identified using the two-part classification scheme applied to nine of the thirty-two stations. It is important to note that signals below the 95th percentile in these global wavelet spectra graphs, despite potential strong alignment with regional cyclic patterns, were not considered discriminatory attributes for classification purposes. For example, if any signal fell below the 95% threshold, no special considerations were given due to potential spatial implications to maintain consistency and subjectivity.

Meteorology **2025**, 4, 29

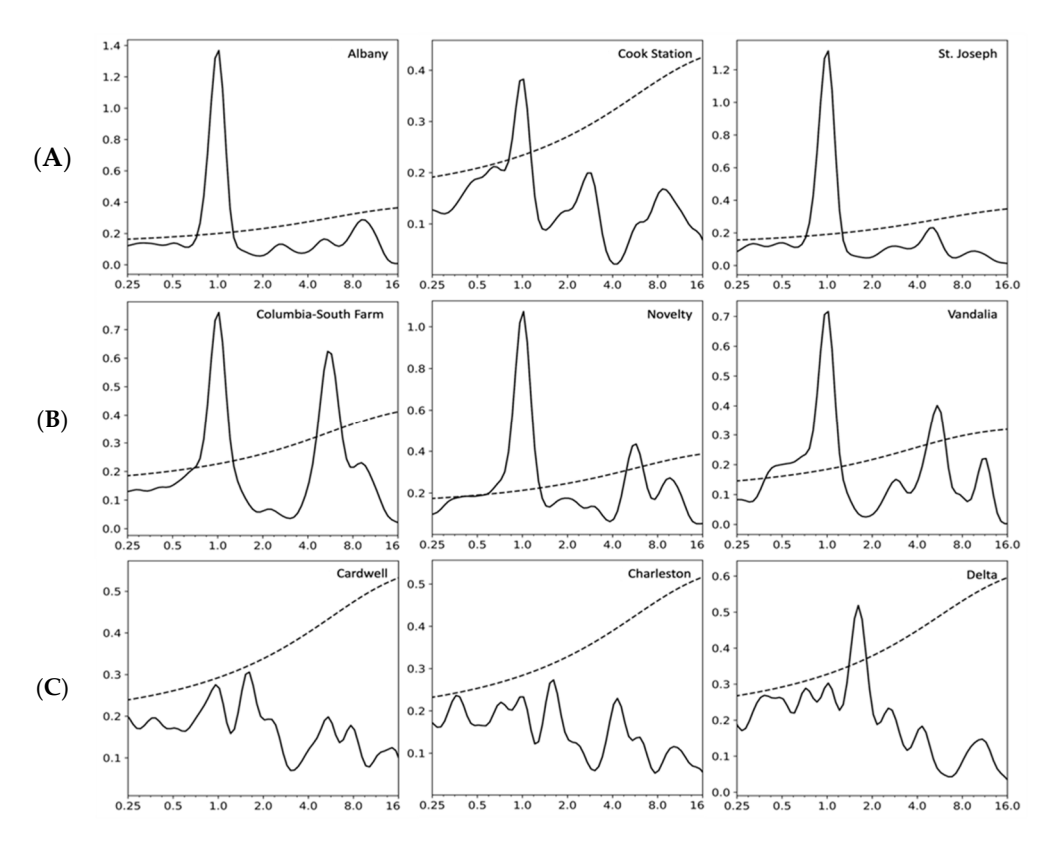


**Figure 5.** Station-based analysis of global wavelet power spectra reveals three classification patterns: top row (**A**), middle row (**B**), and bottom row (**C**). The abscissa represents the period in years and the ordinate is wavelet power (unit is inch<sup>2</sup>). The solid line is wavelet power and the dashed line is the 95% confidence level.

Each station's county, cone of influence (COI), peak period(s), sub-classification, and classification are found in Table 2. According to the station information, the COI column, denoting the largest potential significant period, is proportional to the length of the dataset available. For this reason, the average time found to capture potential ENSO signals was 23 years, with 21 of the 32 stations having a full 25-year period. The maximum potential period that fell within the cone of influence for each station is found in the COI column, with an average of 5.84 years. Although the overall average falls short of the classification range of 2–7 years for ENSO, 28 of the 32 stations did have COIs that extended beyond 7 years. The peak period column identifies any significant peaks within the COI. The average peak of stations that fell into a B classification was 5.48 years. In the ENSO classification scheme, removing Lamar as an outlier (3.34 years), the average peak period was 5.61 years. Of the 32 classifications, 11 fell in the A, 14 in the B, and 7 in the C categories, respectively.

The spatial distribution of classifications across Missouri, when viewed in conjunction with climate divisions, provided an illustrative analysis and highlighted the continuous areas of homogeneous classified stations. For the contextual clarity of augmenting the airport ASOS station datasets, the first map (Figure 6) described will be the four-ASOS-station mapping scheme. The Columbia Regional and St. Louis International airports were classified as falling into region A and the Kansas City International and Springfield-Branson National airports into region B. For illustrative purposes, the ASOS station pattern shapes have been filled. The two regions, which will now be used to delineate two precipitation zones, halve the state into an approximate western zone (A) and eastern zone (B). The western portion of the state (climate divisions 1, 3, and 4) displays a region with precipitation patterns devoid of ENSO influences. Climate divisions 2, 5, and 6, with

Meteorology 2025, 4, 29 11 of 17

precipitation patterns with an ENSO signal, comprise the eastern portion of the state. In this case, with only four stations, no station fell in category C.

**Table 2.** Classification results of the wavelet analysis for Missouri stations, based on cone of influence (COI) and peak period(s). Includes county, sub-classification, and final classification.

Location	County	COI	Peak Period(s)	Sub-Class	Class
Albany	Gentry	9.14	Annual	A	A
Auxvasse	Audrain	9.14	Annual, 5.76	E	В
Brunswick	Carroll	9.10	Annual	A	A
Cardwell	Dunklin	9.14	None	H	C
Charleston	Mississippi	9.14	None	H	C
Clarkton	Dunklin	8.92	None	H	C
Columbia—BREC	Boone	5.73	Annual, 5.43	E	В
Columbia—JFG	Boone	6.04	Annual, 5.43	E	В
Columbia—Sanborn	Boone	9.14	Annual, 5.43	E	В
Columbia—South Farm	Boone	9.14	Annual, 5.43	E	В
Cook Station	Crawford	9.14	Annual	A	A
Corning	Atchison	9.14	0.34, annual	G	A
Delta	Cape Girardeau	9.14	1.62	C	C
Glennonville	Dunklin	9.14	Annual, 1.62	F	A
Green Ridge	Pettis	7.40	Annual, 5.76	E	В
Hayward	Pemiscot	8.99	None	H	C
Lamar	Barton	9.14	0.48, annual, 3.84	E/G	В
Linneus	Linn	9.14	Annual	A	A
Monroe City	Monroe	8.99	Annual, 5.76	E	В
Mountain Grove	Wright	6.28	0.48, annual	G	A
Novelty	Knox	9.14	Annual, 5.76	E	В
Portageville	Pemiscot	9.14	1.62	C	C
Round Spring	Shannon	6.97	Annual	A	A
St. Joseph	Buchanan	9.14	Annual	A	A
Steele	Pemiscot	9.13	None	H	C
Vandalia	Audrain	5.73	Annual, 5.43	E	В
Versailles	Morgan	7.58	Annual, 5.76	E	В
Williamsburg	Callaway	6.82	0.68, annual, 5.76	E/G	В
Columbia NWS	Boone	9.14	Annual, 5.43	E	В
Kansas City NWS	Platte	9.14	Annual	A	A
Springfield NWS	Greene	9.14	0.51, annual	G	A
Saint Louis NWS	St. Louis	9.14	Annual, 5.76	E	В

The subjective alignment of the precipitation zones to the climate divisions is roughly aligned due to spatial uncertainty. The limitations of data-sparse regions were caught in the underlying spatial uncertainty metrics, with a distance that ranged between 0 and 2.5 degrees (Figure 7). Climate divisions 5 and 6 and the northern portion of divisions 1 and 2 had the highest spatial uncertainty (white circles) and the highest certainty in divisions 2 and 4. Given the uncertainty, the interpolation analysis reliability is limited to subjective regional assessments for each station. Although there is balance in the proportion of classification outcomes, the classification methodology would be questionable given only four stations. With the 28 additional Mesonet stations, interpolated data further captured a granular representation of precipitation zones.

Meteorology **2025**, 4, 29

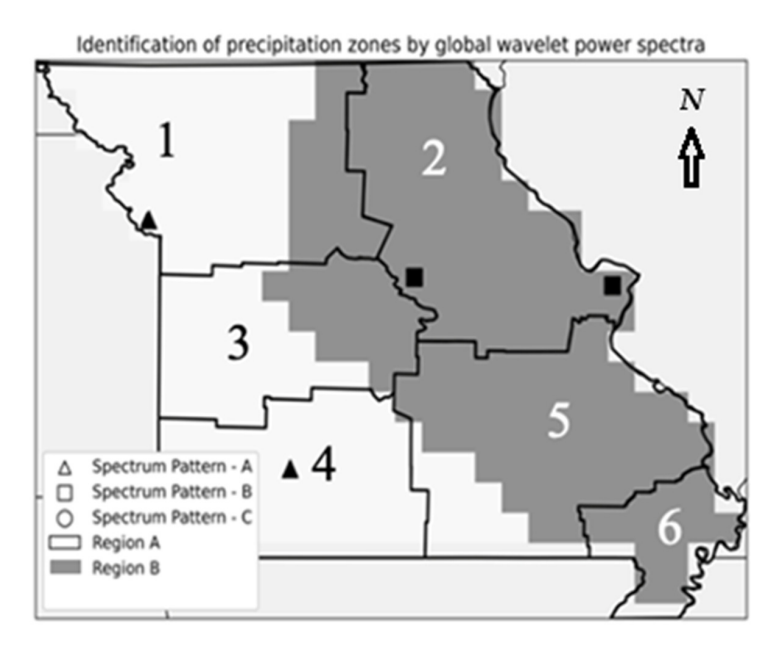


**Figure 6.** Identification of precipitation zones in Missouri using global wavelet power spectra for the four ASOS stations mapping scheme. The mapping results delineate Regions A and B with corresponding spectrum patterns (A and B) shown by symbols. There were no C spectrum patterns found for this mapping scheme. Filled symbols highlight the airport stations for comparison with future Mesonet data analysis. The climate zones (1–6) were adapted from the classification of Missouri climate by the National Climatic Data Center (see [31]). In this map the scale is 1.75 cm = 100 km.

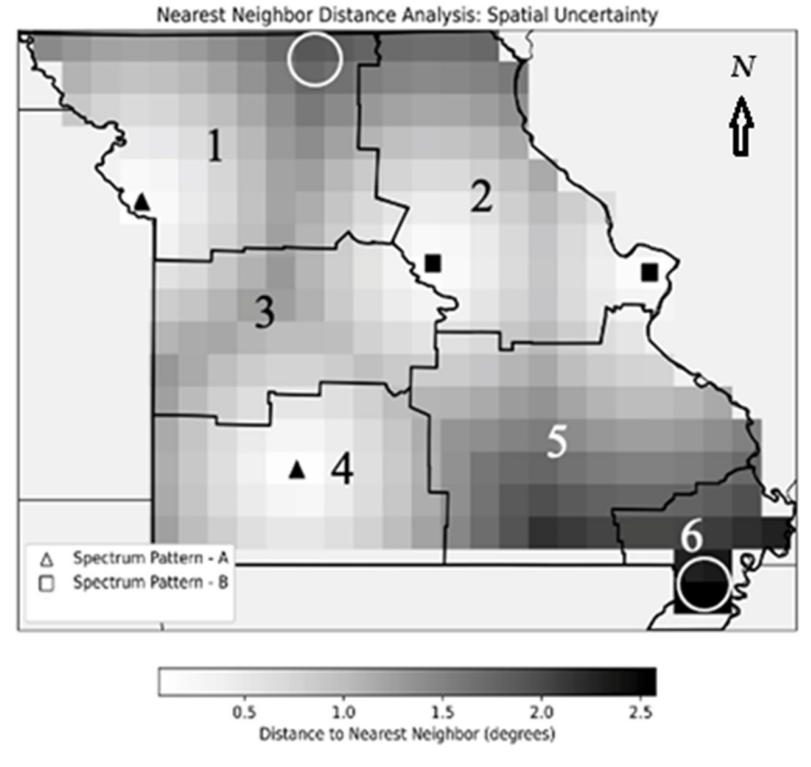


**Figure 7.** Spatial uncertainty of precipitation patterns in the four ASOS station mapping schemes, visualized through nearest-neighbor distance analysis. The grayscale map represents distances (in degrees) to the closest station with a similar pattern, with symbols denoting spectrum patterns A and B. The white circles indicate regions of highest spatial uncertainty. The climate zones (1-6) were adapted from the classification of Missouri climate by the National Climatic Data Center (see [31]). In this map the scale is 1.75 cm = 100 km.

Meteorology **2025**, 4, 29 13 of 17

Augmenting the ASOS station data with Mesonet data provides a new look at precipitation across the state, which has been previously undocumented. Significantly, it is important to note that the Mesonet data classification matches the regional classifications found in the four-ASOS-station mapping scheme. Unlike the four ASOS station precipitation maps that were characterized by two extensive, contiguous multipolygons aligned along a north–south axis, the augmented map depicts four distinct regions. Based on the spatial distribution of global wavelet power spectra (Figure 8), the identified precipitation zones (A, B, C) demonstrate a concordance with the state's recognized geographic climate divisions (1–6). Precipitation zone A comprised two regions, one in climate division 1 (northwest) and the second in climate divisions 4 and 5 (south-central). Precipitation zone B comprised a single region primarily in climate divisions 2 and 3. A station in the northwest of climate division 4 further elongated the region to the southwest. Zone B was notably diagonal, cutting through the central portion of the state in a northeast-to-southwest configuration. Precipitation zone C was predominantly in the very southeast of the state, residing in primarily climate division 6.

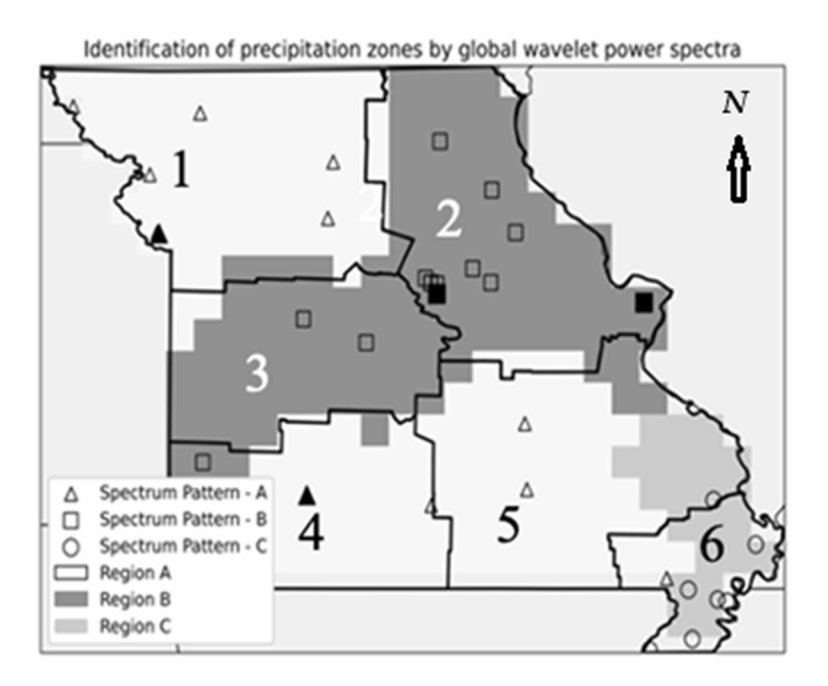


**Figure 8.** Identification of precipitation zones in Missouri using global wavelet power spectra for the augmented mapping scheme (four airports and Mesonet stations). The mapping results delineate regions A, B, and C with corresponding spectrum patterns (A, B, C) shown by symbols. Filled symbols highlight the ASOS stations for comparison with future Mesonet data analysis. The climate zones (1–6) were adapted from the classification of Missouri climate by the National Climatic Data Center (see [31]). In this map the scale is 1.75 cm = 100 km.

Although there are six times as many sources of data for the augmented interpolation, gaps in the spatial data still posed areas of greater uncertainty (Figure 9). Observing the areas of uncertainty, with a few exceptions, the distribution of additional stations renders a map with an overall lower level of uncertainty. The distances of spatial uncertainty over the map are from 0 to 1 degree. The white circle indicates bull's eyes of uncertainty on the order of 1 degree and can be found south of the Kanas City in the Cass County area and south of St. Louis in the St. Francois area. Additional information in the Cass County region could further codify this diagonal feature (precipitation zone B), whereas additional information south of St. Louis could delineate precipitation zone C from zone A in climate division 5.

Meteorology **2025**, 4, 29

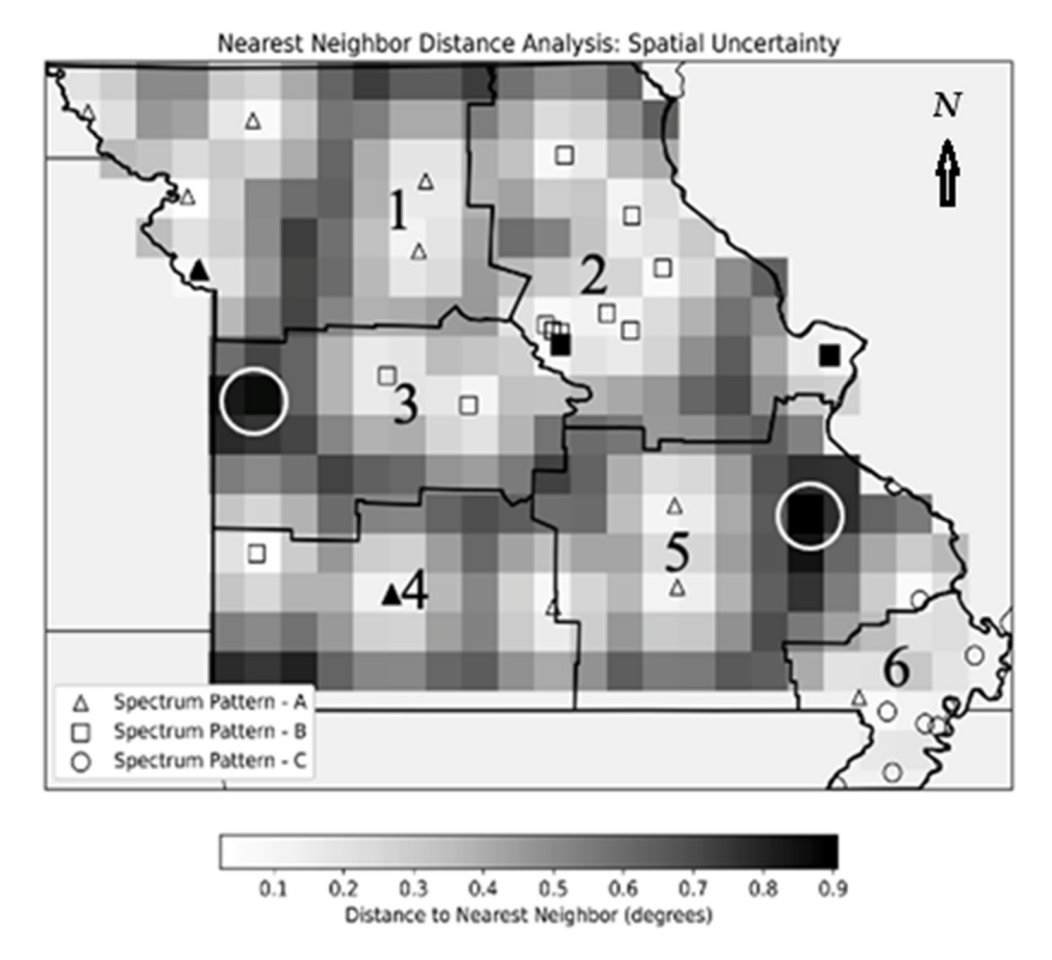


**Figure 9.** Spatial uncertainty of precipitation patterns in the augmented mapping scheme (four ASOS and Mesonet stations), visualized through nearest-neighbor distance analysis. The grayscale map represents distances (in degrees) to the closest station with a similar pattern, with symbols denoting spectrum patterns A, B, and C. The white circles indicate regions of highest spatial uncertainty. The climate zones (1–6) were adapted from the classification of Missouri climate by the National Climatic Data Center (see [31]). In this map the scale is 1.75 cm = 100 km.

By comparing the two mapping schemes, the spatial metrics in Tables 2 and 3 demonstrated that increasing data point density across the state greatly enhances the granular representation of spatial qualities from ground-based sensors. With the addition of the 28 Mesonet stations, there was a 19.58% coverage increase statewide, using the quarter-degree uniform grid and threshold. Spatial overlap between climate divisions 1 and 6 diminished the incremental coverage provided by the additional stations. The total average distance between stations decreased from 105.96 km to just 40.91 km. The standard deviation decreased by 63% from the four-airport station scheme to the augmented scheme, with a decrease in variance of 87%. These results indicate that the station coverage was more uniform, providing an increase in spatial accuracy and resolution. A substantial reduction in minimum and maximum distances again points to the increase in data density. Ultimately, the reduced interquartile distance (IQD) signifies that distances are more tightly clustered around the median in the scheme with additional stations. This indicates a decrease in overall variability and more uniform data distribution.

Meteorology **2025**, 4, 29 15 of 17

**Table 3.** Spatial analysis metrics for the two mapping schemes, comparing four ASOS stations to 32 combined ASOS and Missouri Mesonet stations. Metrics include coverage percentage, average distance, standard deviation, variance, minimum, maximum, and interquartile distances, illustrating the impact of station density on spatial representation.

Spatial Metrics	Four ASOS Stations	32 ASOS + Mesonet
Coverage (%)	3.44	23.02
Average total distance (km)	105.96	40.91
Standard dev. dist. (km)	53.97	19.73
Variance distance (km <sup>2</sup> )	2913.17	389.46
Minimum distance (km)	6.88	2.17
Maximum distance (km)	283.21	90.79
Interquartile distance (km)	74.24	30.18

## 4. Conclusions

This paper sought to show the benefits of augmenting NWS airport ASOS weather station precipitation data with Mesonet station data to better depict climatological signals in precipitation patterns across Missouri. Previous studies have used datasets that were spatially and temporally coarse compared to those used here and studied using Fourier analysis techniques. The resulting regional precipitation insights that were derived from the Mesonet data were both consistent with the airport ASOS station data and revealed spatial details that were not captured in the ASOS data alone.

Using the wavelet method to classify and illustrate station precipitation patterns has proved successful. Not only were there distinct signals in the precipitation data, but these signals fell within known cyclic patterns. Despite temporal constraints on discernible signal length due to limited sample sizes, the nearly 25 years of Mesonet station data offered a sufficient sample for ENSO length diagnostics. In time, this analysis will render an increasingly better depiction of the spatial characteristics of precipitation patterns as station records increase.

The results of this analysis provided a subjective look at precipitation sensitivity with regard to annual and ENSO signals. It does not, however, indicate that one precipitation zone receives more precipitation than another. Rather, the zones denote regions where the precipitation patterns have aligned with an annual or ENSO signal or neither. This study lacked direct temporal evaluations for deriving specific ENSO phase-related attributes. Rather, by detrending and normalizing the station data, there was a focus on the precipitation patterns, not fluctuations of the absolute amounts. Therefore, if prolonged droughts and above-average precipitation season(s) are driven by similar cyclic trajectories, their power spectra would be similar. This implies that this specific study does not address the nuances of precipitation amount to ENSO phases, strength, or duration.

Instead, this global wavelet spectrum analysis provided a method to cut through temporal nuances of each station and summarize the location broadly. The analysis showed a diagonal precipitation zone running northeast to the southwest flank by two regions marked by precipitation driven primarily due to an annual signal. The classification relegated stations lacking statistically significant annual or ENSO signals to a residual category, with these stations clustering in the furthest southeast region, the bootheel portion of the state.

Future considerations concerning the effectiveness and utility of the wavelet to identify precipitation signals abound. Using the global wavelet spectrum alone masks the discrete patterns over the time series observed in the scalogram. This specific analysis employed a Morlet (6) 'mother' wavelet, chosen for its optimal balance between temporal and power resolution. Smaller wavelet scales, corresponding to higher-frequency components, re-

Meteorology **2025**, 4, 29 16 of 17

vealed two distinct periods of strongest average temporal power related to ENSO across all categorized stations: approximately 2006–2013 and 2015–2024. A cross-wavelet transform of the locations that had this 'ENSO-like' signal was used to further evaluate these time periods. The results supported that during this time period, both ENSO and precipitation were either directly in-phase or slightly leading, suggesting that strong ENSO variability coincided with the dominant precipitation patterns during this time. Future research could reveal that linking precipitation zones sensitive to ENSO changes may enable more focused regional efforts to anticipate areas most impacted by climate change across the state. Additionally, this methodology could be extended to future comparative studies in diverse mid-latitude regions, including parts of Europe, Central Asia, or southern Brazil. Such research aims to determine if similar regional precipitation clusters associated with intrinsic cyclic behavior emerge.

**Author Contributions:** Conceptualization, J.J.S. and A.R.L.; methodology, J.J.S.; software, J.J.S.; validation, J.J.S.; formal analysis, J.J.S.; investigation, J.J.S. and A.R.L.; resources, J.J.S.; data curation, J.J.S.; writing—original draft preparation, J.J.S.; writing—review and editing, J.J.S. and A.R.L.; visualization, J.J.S.; supervision, A.R.L.; project administration, A.R.L. All authors have read and agreed to the published version of the manuscript.

**Funding:** This research received no external funding.

**Institutional Review Board Statement:** Not applicable.

**Informed Consent Statement:** Not applicable.

**Data Availability Statement:** The data presented in this study are available on request from the corresponding author. The data are not publicly available due to privacy.

**Acknowledgments:** The authors would like to thank the three anonymous reviewers for their time and constructive comments. These comments improved the paper.

Conflicts of Interest: The authors declare no conflicts of interest.

#### References

- 1. Missouri Historical Agricultural Weather Database. Available online: http://agebb.missouri.edu/weather/stations/ (accessed on 1 October 2025).
- 2. Birk, K.; Lupo, A.R.; Guinan, P.E.; Barbieri, C.E. The interannual variability of Midwestern temperatures and precipitation as related to the ENSO and PDO. *Atmosfera* **2010**, 23, 95–128.
- 3. Lupo, A.R.; Smith, S.N.; Guinan, P.E.; Chesser, M.D. The climatology of Missouri Region dew points and the relationship to ENSO. *Natl. Weather Dig.* **2012**, *36*, 10–20.
- 4. Henson, C.B.; Lupo, A.R.; Market, P.S.; Guinan, P.E. ENSO and PDO-related climate variability impacts on Midwestern United States crop yields. *Int. J. Biometeorol.* **2017**, *61*, 857–867. [CrossRef]
- 5. Lupo, A.R.; Kononova, N.K.; Semenova, I.G.; Lebedeva, M.G. A comparison of the characteristics of extreme drought during the late 20th and early 21st centuries over Eastern Europe, Western Russia, and Central North America. *Atmosphere* **2021**, *12*, P01033. [CrossRef]
- Cook, A.R.; Leslie, L.M.; Parsons, D.B.; Schaefer, J.T. The impact of El Niño–Southern Oscillation (ENSO) on winter and early spring U.S. tornado outbreaks. J. Appl. Meteorol. Clim. 2017, 56, 2455–2478. [CrossRef]
- 7. Rasmusson, E.M.; Mo, K.-C. Linkages between 200-mb tropical and extratropical circulation anomalies during the 1986–1989 ENSO cycle. *J. Clim.* **1993**, *6*, 595–616. [CrossRef]
- 8. Cook, A.R.; Schaefer, J.T. The relation of El Niño–Southern Oscillation (ENSO) to winter tornado outbreaks. *Mon. Weather Rev.* **2008**, *136*, 3121–3137. [CrossRef]
- 9. NOAA/CPC, 2023: ENSO Related Winter Features over North America. Available online: https://www.cpc.ncep.noaa.gov/products/analysis\_monitoring/ensocycle/nawinter.shtml (accessed on 1 October 2025).
- 10. Wang, Y.; Lupo, A.R. An extratropical air-sea interaction over the North Pacific in association with a preceding El Niño episode in early summer. *Mon. Weather Rev.* **2009**, 137, 3771–3785. [CrossRef]
- 11. Zhao, P.; Cao, Z.; Chen, J. A summer teleconnection pattern over the extratropical Northern Hemisphere and associated mechanisms. *Clim. Dyn.* **2010**, *35*, 523–534. [CrossRef]

Meteorology **2025**, 4, 29 17 of 17

12. Wang, Y.; Lupo, A.R.; Qin, J. A response in the ENSO cycle to an extratropical forcing mechanism during the El Niño to La Niña transition. *Tellus Ser. A Dyn. Meteorol. Oceanogr.* **2013**, *65*, 22431. [CrossRef]

- 13. Lupo, A.R.; Mokhov, I.I.; Chendev, Y.G.; Lebedeva, M.G.; Akperov, M.; Hubbart, J.A. Studying summer season drought in western Russia. *Adv. Meteorol.* **2014**, 2014, 942027. [CrossRef]
- 14. Cherenkova, E.; Semenova, I.; Bardin, M.; Zolotokrylin, A.N. Drought and grain crop yields over the East European Plain under influence of quasibiennial oscillation of global atmospheric processes. *Int. J. Atmos. Sci.* 2015, 932474. [CrossRef]
- 15. Wang, N.; Zhang, Y. Evolution of Eurasian teleconnection pattern and its relationship to climate anomalies in China. *Clim. Dyn.* **2015**, *44*, 1017–1028. [CrossRef]
- 16. Santos, C.A.G.; de Morais, B.S. Identification of precipitation zones within São Francisco River basin (Brazil) by global wavelet power. *Hydrol. Sci. J.* **2013**, *58*, 789–796. [CrossRef]
- 17. Singh, J.; Ashfaq, M.; Skinner, C.; Anderson, W.; Mishra, V. Enhanced risk of concurrent regional droughts with increased ENSO variability and warming. *Nat. Clim. Change* **2022**, *12*, 163–170. [CrossRef]
- 18. Berenyi, A.; Bartholy, J.; Pongracz, R. Analysis of precipitation-related climatic conditions in European plain regions. *Weather Clim. Extrem.* **2023**, *42*, 100610. [CrossRef]
- 19. Platikanov, S.; Lopez, J.F.; Martrat, B.; Martin-Vide, J.; Tauler, R. Temporal and spatial relationships between climatic indices and precipitation zones in Europe, Spain and Catalonia. *Int. J. Clim.* **2024**, *45*, e8699. [CrossRef]
- Nazeri Tahroudi, M. Comprehensive global assessment of precipitation trend and pattern variability considering their distribution dynamics. Nat. Sci. Rep. 2025, 15, 22458. [CrossRef]
- 21. Torrence, C.; Compo, G.P. A practical guide to wavelet analysis. Bull. Am. Meteorol. Soc. 1998, 79, 61–78. [CrossRef]
- 22. Mahdade, M.; Le Moine, N.; Moussa, N.; Navratil, R.; Ribstein, O.; Pierre, P. Automatic identification of alternating morphological units in river channels using wavelet analysis and ridge extraction. *Hydrol. Earth Syst. Sci.* **2020**, *24*, 3513–3537. [CrossRef]
- 23. Farge, M. Wavelet transforms and their applications to turbulence. Annu. Rev. Fluid Mech. 1992, 24, 395–457. [CrossRef]
- Keener, V.W.; Feyereisen, G.W.; Lall, U.; Jones, J.W.; Bosch, D.D.; Lowrance, R.R. El-Niño Southern Oscillation (ENSO) influences on monthly NO<sub>3</sub> load and concentration, stream flow and precipitation in the Little River Watershed, Tifton, GA. J. Hydrol. 2010, 381, 352–363. [CrossRef]
- 25. Nakken, M. Wavelet analysis of rainfall-runoff variability isolating climatic from anthropogenic patterns. *Environ. Model. Softw.* **1999**, *14*, 283–295. [CrossRef]
- 26. Midwest Regional Climate Center. Available online: https://mrcc.purdue.edu/ (accessed on 15 February 2025).
- 27. Campbell Scientific—Rain Gage with 6-Inch Orifice. Available online: https://www.campbellsci.com/te525-et (accessed on 5 February 2025).
- 28. Li, J.; Heap, A.D. A review of spatial interpolation methods for environmental sciences. In *A Report for Geoscience Australia*; Geoscience Australia: Canberra, ACT, Australia, 2008; p. 155, ISBN 978-1-921498-30-5.
- 29. Bosch, M. Swisslandstats-geopy: Python tools for the land statistics datasets from the Swiss Federal Statistical Office. *J. Open Source Softw.* **2019**, *4*, 1511. [CrossRef]
- 30. Vincenty, T. Direct and inverse solutions of geodesics on the ellipsoid with application of nested equations. *Surv. Rev.* **1975**, 23, 88–93. [CrossRef]
- 31. NCDC. Climate of Missouri. National Oceanic and Atmospheric Administration. 2006. Available online: https://www.ncei.noaa.gov/access/monitoring/reference-maps/conus-climate-divisions (accessed on 22 September 2025).

**Disclaimer/Publisher's Note:** The statements, opinions and data contained in all publications are solely those of the individual author(s) and contributor(s) and not of MDPI and/or the editor(s). MDPI and/or the editor(s) disclaim responsibility for any injury to people or property resulting from any ideas, methods, instructions or products referred to in the content.